A unique virus release mechanism in the Archaea

Ariane Bize[a], Erik A. Karlsson[b], Karin Ekefjärd[b], Tessa E. F. Quax[a], Mery Pina[a], Marie-Christine Prevost[c], Patrick Forterre[a], Olivier Tenaillon[d], Rolf Bernander[b], and David Prangishvili[a,1]

[a]Biologie Moléculaire du Gène chez les Extrêmophiles and [c]Plate-Forme de Microscopie Ultrastructurale, Institut Pasteur, 25 rue du Docteur Roux, 75724 Paris cedex 15, France; [b]Department of Molecular Evolution, Evolutionary Biology Center, Uppsala University, Norbyvägen 18C, SE-752 36 Uppsala, Sweden; and [d]Institut National de la Santé et de la Recherche Médicale, Unité 722, Faculté de médecine Xavier Bichat, Université Paris 7, 16 rue Henri Huchard, 75018 Paris, France

Edited by Carl R. Woese, University of Illinois, Urbana, IL, and approved May 14, 2009 (received for review February 4, 2009)

Little is known about the infection cycles of viruses infecting cells from Archaea, the third domain of life. Here, we demonstrate that the virions of the archaeal *Sulfolobus islandicus* rod-shaped virus 2 (SIRV2) are released from the host cell through a mechanism, involving the formation of specific cellular structures. Large pyramidal virus-induced protrusions transect the cell envelope at several positions, rupturing the S-layer; they eventually open out, thus creating large apertures through which virions escape the cell. We also demonstrate that massive degradation of the host chromosomes occurs because of virus infection, and that virion assembly occurs in the cytoplasm. Furthermore, intracellular viral DNA is visualized by flow cytometry. The results show that SIRV2 is a lytic virus, and that the host cell dies as a consequence of elaborated mechanisms orchestrated by the virus. The generation of specific cellular structures for a distinct step of virus life cycle is known in eukaryal virus-host systems but is unprecedented in cells from other domains.

lysis | virus factory | hyperthermophile | infection cycle

As for organisms belonging to the Bacteria and Eukarya, members of the domain Archaea are infected by specific viruses. The majority of archaeal viruses isolated so far contain dsDNA as the genetic material and infect hyperthermophilic hosts from the phylum Crenarchaeota (1). The diversity and uniqueness of these viruses at both the morphological and genetic levels are such that they have been classified into 7 viral families (2). The knowledge on the biology of this exceptional group of viruses is still limited, partly because of the unique genetic content: very few genes have detectable functions or homologs in the databases (3).

In particular, little is known about relationships of crenarchaeal viruses with their hosts. Except for a few isolated cases (4–6), it is generally presumed that these viruses persist in the host cell in a carrier state, a nonlytic relationship in which virions are continuously secreted by the still-dividing cells (7). However, the classification of crenarchaeal viruses as chronic is based on indirect experimental evidence, such as a lack of optical density (OD) decrease and absence of cellular debris in infected cultures (e.g., 8, 9). Detailed characterization of the infection cycle and the carrier state has not been specifically addressed in the scarce reports on crenarchaeal host-virus interactions (see e.g., 10).

To study the nature of host-virus relationships in crenarchaea, we selected the nonenveloped, rod-shaped virus SIRV2 and its hyperthermophilic and acidophilic host, *Sulfolobus islandicus*. SIRV2, originally described as a carrier state, nonlysogenic virus (11), belongs to a common crenarchaeal virus family, the *Rudiviridae* (9, 11, 12, 13, 14), and contains a linear 35.5-kb dsDNA genome (15). The host belongs to a well characterized crenarchaeal genus, *Sulfolobus* (16, 17), from which also other viruses are known (2). We describe detailed in vivo effects of the virus on its host and, unexpectedly, demonstrate that SIRV2 is a cytocidal, lytic virus. Remarkably, a unique virus release mechanism was encountered during the characterization, involving the generation of pyramidal structures that, by opening out, cause local disruption of the cell envelope and allow virion escape. In addition, intracellular viral DNA was visualized by flow cytometry, and the technique was also used to demonstrate chromosome degradation in infected cells.

Results

Growth Kinetics of SIRV2-Infected Cultures. OD and CFU values from uninfected and infected [multiplicity of infection (moi) ≈7] cultures of *S. islandicus* were monitored over time. The effects of the virus were visible already 1.5 h after infection (Fig. 1). Whereas uninfected cultures pursued normal growth with a generation time of ≈13 h, the OD in infected cultures remained constant for ≈60 h (Fig. 1 *A* and *C*), after which growth resumed (Fig. 1*C*). During this time period, the CFU values of uninfected controls remained constant or increased slightly. In contrast, the CFU values decreased dramatically in infected cultures, resulting in an ≈1,000-fold reduction at 6 h after infection (Fig. 1*B*, 10.5 h). The CFU values also revealed growth of a minor cell population in infected cultures starting at early time points (Fig. 1*D*, from 15 h). This growth was initially not detectable in the OD measurements (Fig. 1*C*), because of the low concentration of this cell population at early time points. Thus, infection by SIRV2 has a pronounced effect on the host cultures, preventing growth of a majority of the cells.

To exclude the possibility that the results were linked to the high moi used, or to the specific growth conditions, similar experiments were performed at low moi ($\approx 10^{-3}$), at different temperatures (70 °C, 75 °C, and 78 °C), pHs (3.0 and 3.5), medium richnesses (standard medium or 5-fold less rich medium), and with different host strains (*S. islandicus* strains KVEM10H3, HVE10/4, and LAL14/1). No significant differences were observed, indicating that the effects occurred independently of these parameters.

The cell population growing in the presence of SIRV2 consisted of cells completely resistant to SIRV2 infection, not producing any detectable infectious virions nor carrying the SIRV2 genome (*SI Text* and Fig. S1). This was consistent with the observation that the SIRV2 genome does not integrate into the host chromosome (11), and excluded the possibility that SIRV2 established a carrier state relationship with its host. The high initial proportion of resistant cells suggested that specific mechanisms could be involved in their generation, in addition to random mutations, such as CRISPR-related mechanisms (18).

Flow Cytometry Analysis of Infected Cells over Time. The cell size and intracellular DNA content in uninfected and SIRV2-infected cultures (moi ≈10) over time were monitored by flow cytometry (Fig. 2, Fig. S2, and Fig. S3).

The relative lengths of the *S. islandicus* cell cycle periods in the control cultures were found to be similar to those of other *Sulfolobus* species (16, 19), with the post-replicative phase occupying a large fraction of the generation time (68%, Fig. S4). Based on comparison of the flow cytometry fluorescence (DNA content)

Author contributions: A.B., O.T., R.B., and D.P. designed research; A.B., E.A.K., K.E., T.E.F.Q., M.P., and M.-C.P. performed research; A.B., E.A.K., M.-C.P., P.F., O.T., R.B., and D.P. analyzed data; and A.B., R.B., and D.P. wrote the paper.

The authors declare no conflict of interest.

This article is a PNAS Direct Submission.

[1]To whom correspondence should be addressed. E-mail: david.prangishvili@pasteur.fr.

This article contains supporting information online at www.pnas.org/cgi/content/full/0901238106/DCSupplemental.

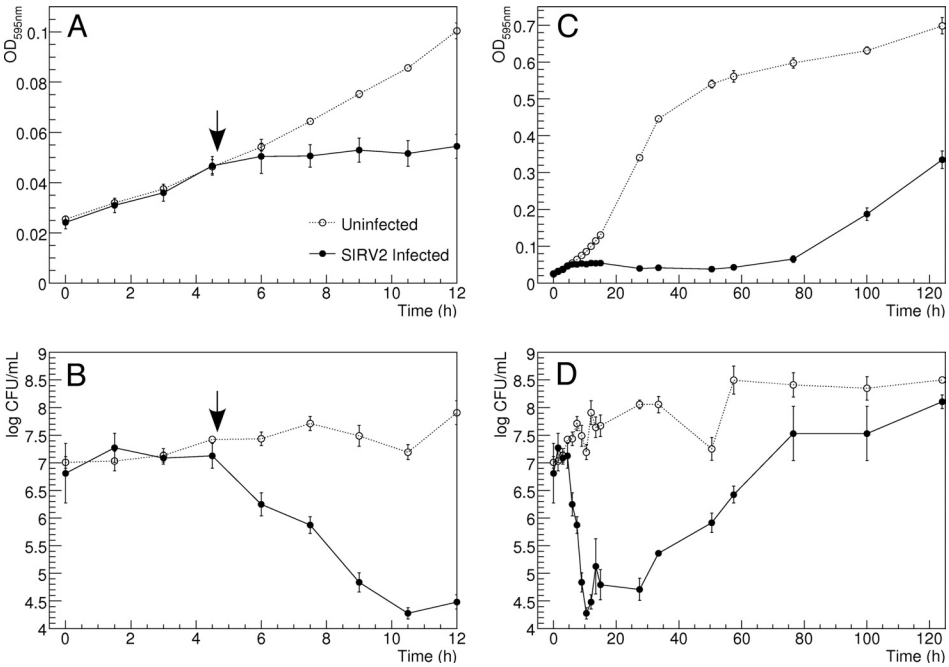

Fig. 1. Impact of SIRV2 infection on the growth kinetics of *S. islandicus* cultures. Cultures infected at a moi of ≈7 (filled circles, continuous line) and uninfected cultures (empty circles, dotted lines), were launched in triplicates. Averages of the replicates ± 1 SD are shown. The vertical arrows in *A* and *B* correspond to virus addition (4.5 h). (*A*) $OD_{595\ nm}$, detail of the first hours. (*B*) Log transformation of the CFU titres, detail of the first hours. (*C*) $OD_{595\ nm}$ over the entire time course. (*D*) Log transformation of the CFU titers over the entire time course.

signals with those from the sequenced genomes of *S. acidocaldarius* and *S. solfataricus*, the genome size was estimated to ≈2.6 Mb (Fig. S5). The average cell size (Fig. 2*A Left* and Fig. S3) progressively decreased when the cultures approached stationary phase. In the infected cultures (Fig. 2*B Left*), a cell size increase initially occurred in part of the cell population, evident as an extension of the distribution toward the right (6–8 h). Subsequently, the average cell size gradually decreased over time.

The DNA content distributions of the control cultures (Fig. 2*A Right* and Fig. S2) were typical for exponentially growing *Sulfolobus* cells (19), with a majority of the cells containing 2 chromosomes. In the infected cultures (Fig. 2*B Right*), cells with a very low DNA content (≪1 genome equivalent) started to appear at 0.5 h after infection and then increased in proportion over time whereas the proportion of cells containing 1–2 genome equivalents decreased. Thus, at 12 h, a large majority of the cell population contained no detectable intracellular DNA. The SIRV2 latent period is 8–10 h (below), and chromosome degradation, thus, occurred before virus release in a significant fraction of the cell population. Interestingly, the populations of chromosome-less cells and cells containing DNA were clearly separated and well defined (Fig. 2*B Right* and Fig. S6). Thus, for a given infected cell, chromosome degradation must have occurred within a brief time interval.

In parallel to chromosome degradation, an increase in the total DNA content occurred in part of the cell population, evident as an extension of the 2-genome equivalents peak toward the right (Fig. 2*B Right*, 2 h and onwards). The increase was (Fig. 2*C*, arrow) estimated to ≈0.5 genome equivalents per cell, or 1.3 Mb, on average 3 h after infection, and it corresponded to newly synthesized viral DNA (below).

The results demonstrate that infection by SIRV2 causes massive degradation of the host chromosome in virtually all infected cells during the first 12 h of infection, excluding the possibility that SIRV2 genomes are vertically transmitted between cell generations.

Links Between the Virus Infection Cycle, the Kinetics of Host Chromosome Degradation, and Cell Death. To discriminate between host chromosome and viral DNA, uninfected and infected cultures (moi ≈15) were monitored by dot blot hybridizations, in addition to flow cytometry. In an uninfected control culture, the percentage of chromosome-less cells did not exceed 5% (Fig. 3*A*) and tended to decrease over time. In infected cultures, chromosome-less cells began to accumulate in the first hours, and after 5 h, the percentage was ≈40%, confirming that significant degradation occurred before virion release (at ≈8–10 h, see below) and, at 11 h, >80% of the cells were chromosome-less. Subsequent degradation occurred at a lower rate and finally reached 97%, confirming that genome degradation occurred in most cells.

The intracellular amount of SIRV2 DNA (Fig. 3 *B* and *D*) increased gradually and reached a maximum after ≈8 h, followed by a large decrease up until 14 h. The initial increase presumably corresponded to viral DNA replication, and the decrease to virus release, indicating a latent period of ≈8–10 h. Thus, a single round of infection occurred in the cultures at the high moi used. To relate viral DNA production to the dynamics of chromosome degradation, the percentage of DNA-less cells appearing between successive time points was superimposed (Fig. 3*B*). A small peak of degradation, visible at 0.5 h after infection, was most likely an artifact caused by the low signal-to-noise ratio for DNA-less cells in the very early time points. The major peak occurred at 11 h, in the middle of the virus release period. The use of a 16S rRNA gene probe combined with similar data analysis confirmed the chromosome degradation observed by flow cytometry (Fig. 3 *C* and *E*).

To confirm the latent period of 8–10 h and to estimate the burst size, a 1-step growth experiment was performed (*SI Text* and Fig. S7). Virus release was shown to begin at ≈8–10 h after infection, confirming that no infectious virions were released before this time point, consistent with all other data. The burst size was estimated to 30 ± 10 viruses per cell. Finally, a membrane potential-sensitive probe (*SI Text* and Fig. S8) was used to confirm that cell death occurred in connection to virus release.

In conclusion, a single round of infection occurred when a high moi was used, and the SIRV2 latent period was ≈8–10 h under the conditions used. Massive host chromosome degradation occurred throughout the infection cycle, starting from the early stage, and cell death took place concomitantly with virus release. Thus, SIRV2 is a lytic virus that kills the host cell during the process of virus production and release.

Identification of Cellular Ultrastructures Induced by SIRV2 Infection. To obtain insights into the details of the virus-host interaction, infected cells were analyzed by SEM and TEM. The cells were fixed

MICROBIOLOGY

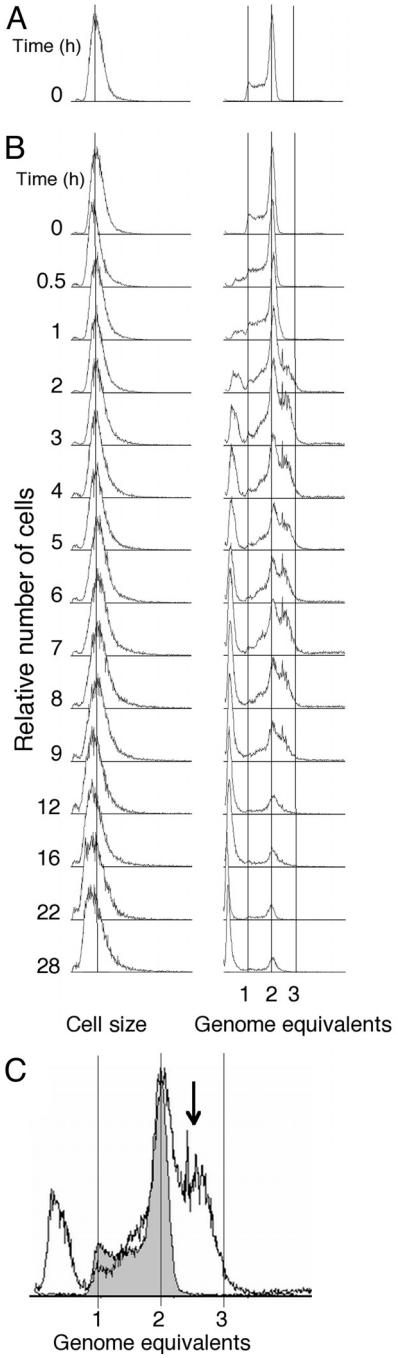

Fig. 2. Flow cytometry time-course analysis of *S. islandicus* cells infected by SIRV2. (*A*) Representative cell size and DNA content distributions from an uninfected culture. (*B*) Cell size and DNA content distributions from a culture infected with SIRV2 (moi ≈10). The virus was added just after time point 0 h. (*C*) Visualization of intracellular SIRV2 DNA by flow cytometry at 3 h after infection. The DNA content distribution from an infected *S. islandicus* culture is shown against the distribution from an uninfected culture (translucent gray). The arrow indicates additional DNA in infected cells.

at 10 h (just before virion release), 13 h (middle of release period), and 26 h (after release) after infection. Uninfected cells in midexponential growth phase were used as control. For analysis with TEM, ultrathin sections of samples were prepared.

The irregular coccoid morphology of uninfected cells was typical for *Sulfolobales* species, with the cell envelope consisting of a lipid membrane and an S-layer (Fig. 4 *A1* and *A2*). At 10 h after infection, multiple pyramidal protrusions were observed on the cell surface by SEM (Fig. 4*B1*, arrows), which were absent in uninfected control cells. In thin sections analyzed by TEM, these structures appeared as large angular protrusions associated with a local absence of S-layer on the cell envelope (Fig. 4 *B2–B4*). Both with SEM and TEM, several such virus-associated pyramids (VAPs) were usually visible per cell (Fig. 4 *B1* and *B2*). The pyramidal structure of the VAPs, suggested by SEM, was confirmed by TEM, showing a polygonal base in a plane parallel to the cell envelope (Fig. 4*B5*). In thin sections, the VAPs often contained regions producing a denser staining (Fig. 4*B2*, arrows), localized at the tip of the pyramidal structure.

Dense aggregates of virions were visible by TEM within numerous cells from the infected culture (examples in Fig. 4 *B4* and *B6*), showing that virion assembly occurred in the cytoplasm. Up to 3 densely packed aggregates, together containing up to ≈150 virions, were detected in the cell sections, and occupied a high fraction of the intracellular volume. The higher number of virions compared with the estimates from the 1-step growth experiment (above) could be due to that virions may still be aggregated after release.

At 13 h after infection, together with cells resembling the examples shown in Fig. 4 *B1* and *B2*, cells lacking VAPs and displaying numerous perforations on the cell surface were observed (similar to Fig. 4 *C1* and *C2*), and 26 h after infection almost all cells were perforated and empty (Fig. 4 *C1* and *C2*). The perforated cells exhibited spherical morphotype, different from the native phenotype, suggesting an altered intracellular organization. Thin section analysis of perforated cells displayed virion remains (Fig. 4*C2 Inset*) and disappearance of most of the cytoplasmic content (Fig. 4*C2*). The cell perforations were heterogeneous in size, and their majority visible in thin sections had a diameter in the range of 200 nm. TEM analysis revealed that the perforations were delimited by C-shaped structures (Fig. 4 *C2* and *C3*), and it is likely that these represented VAP remains. Apart from the perforations, the cell envelope appeared to be intact, with both the S-layer and the membrane visible (Fig. 4 *C2* and *C3*). Notably, the characteristic structures at the boundary of the perforations of the lysed cells were sometimes observed detached from the cell envelope (Fig. 4 *C4–C6*). The resemblance of polygonal shapes in Fig. 4 *B5*, *C5*, and *C6*, as well as the similarity of the structures in Fig. 4 *B3* and *C3*, supports the hypothesis that the structures in Fig. 4*C* represented remains of the VAPs shown in Fig. 4*B*. Thus, the VAPs were apparently involved in perforation of the cell envelope. Because ongoing virus release could not be detected, this must have occurred within a brief time interval.

Discussion

We report a detailed cellular study of the infection cycle of a crenarchaeal virus and demonstrate that SIRV2 is a lytic virus. The virions are assembled in the cytoplasm of the host cell and, 8–10 h after infection, start to be released through well defined apertures in the cell envelope. Remarkably, formation of these openings is preceded and facilitated by the generation of virus-induced cellular structures of pyramidal shape, VAPs, located at the cell envelope and pointing outwards. The VAPs perforate the membrane and S-layer, and after disruption leave behind apertures delimited by a ring structure of polygonal shape. After virion release, the cell envelope remains as a stable empty shell. Intracellular viral DNA was visualized by flow cytometry, and the same technique was used to show that host chromosome is completely degraded during the viral infection cycle. The combination of the data from 1-step growth experiment, flow cytometry, and TEM showed that chromosome degradation most likely occurred before virion release, in the majority of the cell population. Together, all of our results demonstrate that the host cells die as a consequence of specific and unique mechanisms orchestrated by the virus, rather than from general deleterious effects of the infection. The deduced viral life cycle is schematically illustrated in Fig. 5.

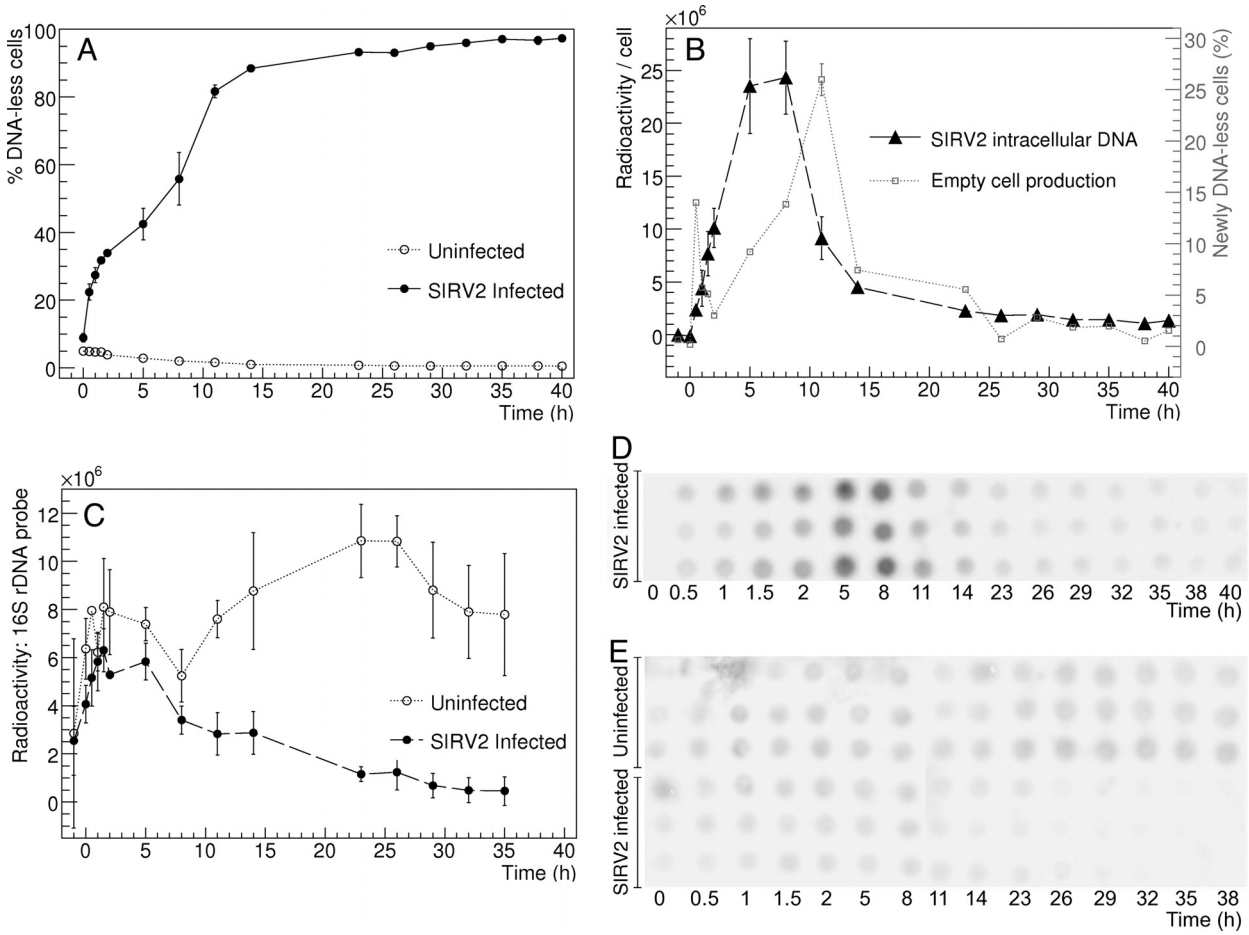

Fig. 3. Links between the kinetics of host chromosome degradation and the SIRV2 infection cycle. Infected cultures and uninfected cultures were launched in triplicates. SIRV2 was added (moi ≈15) just after time point 0 h. Averages of 3 infection replicates ± 1 SD are shown in *A*–*C*. (*A*) Percentage of DNA-less cells in uninfected and infected cultures. The values were obtained by flow cytometry analysis, using data from 2-parameter distributions, gating them as illustrated in Fig. S6*B*. (*B*) Radioactivity/cell (filled triangles, discontinuous line, left axis), indicative of SIRV2 intracellular DNA in infected cultures, over a time course. Values in arbitrary units were obtained by quantifying the hybridization signal from each spot in the image shown in *D*. The percentage of DNA-less cells appearing between 2 successive time points (empty circles, dotted line, right axis) was also plotted, using the data from *A*. (*C*) Radioactivity/cell indicative of intracellular 16S rDNA amounts in uninfected cultures (empty circles, dotted line) or infected cultures (filled circles, discontinuous line). Values in arbitrary units were obtained by quantifying the hybridization signal from each spot in the image shown in *E*. (*D*) Autoradiogram of hybridization of spots of cells sampled from infected cultures with a SIRV2-specific probe. Each spot corresponds to the same approximate number of cells, based on OD measurements. The time course corresponds to horizontal lines, with the 3 replicates shown vertically for each time point. (*E*) Autoradiogram of hybridization of spots of cells sampled from uninfected and infected cultures with a 16S rRNA gene-specific probe. See *D* for additional explanations.

It is likely that a set of viral genes must control the formation of the VAPs and the generation of the apertures through which the virions are released. The genes might either directly code for the proteins involved or modulate host-encoded mechanisms. The timing of VAP disruption and virus release must also be controlled by virus-encoded functions, such that cell lysis does not occur until the virions have been assembled, as for any lytic virus. Further, host chromosome degradation could also be an active mechanism, encoded by viral genes.

To our knowledge, the virus release mechanism identified here is unprecedented in virus biology. In lytic bacteriophages, the 2 main lysis strategies rely on the direct degradation of peptidogycan, for example, with the holin-endolysin system (20), or on the inhibition of cell wall synthesis (21). Both strategies result in complete cell disruption, and do not involve a modification of the cell envelope in several localized regions, as reported here. Also for eukaryotes there are no reports, to our knowledge, on generation of distinct structures for cell perforation and viral release. Modification of intracellular membranes (endoplasmic reticulum, Golgi complex) does occur as a result of infection with certain eukaryotic RNA and DNA viruses, but this appears to be linked to viral replication rather than release (22). Recently, alteration of the *Sulfolobus* S-layer as a result of infection with the lytic icosahedral STIV virus was reported (23). It would be highly interesting if viruses that display little similarity in morphology and gene content would share a related mechanism for extrusion from the host cell.

The number and extent of elaborate modifications caused by SIRV2 on the host cell result in a radically transformed cell that can hardly be contemplated as the archaeon *Sulfolobus*. The whole infected cell rather appears to be converted into a complex viral factory, conceptually identical to those built by some eukaryotic viruses inside infected cells. In such cases, the structures of the factory are enclosed by a membrane to exclude cellular organelles. Ribosomes are, however, present, and the factory is dedicated to viral genome replication and virion assembly (24, 25). The eukaryotic viral factories were suggested to constitute the genuine identity of viruses (26), which thus might be considered as a specific type of living organisms (26, 27). A weakness of this concept was the failure to observe viral factories in cells from other domains. SIRV2, as described above, constitutes an example of archaeal virus producing

MICROBIOLOGY

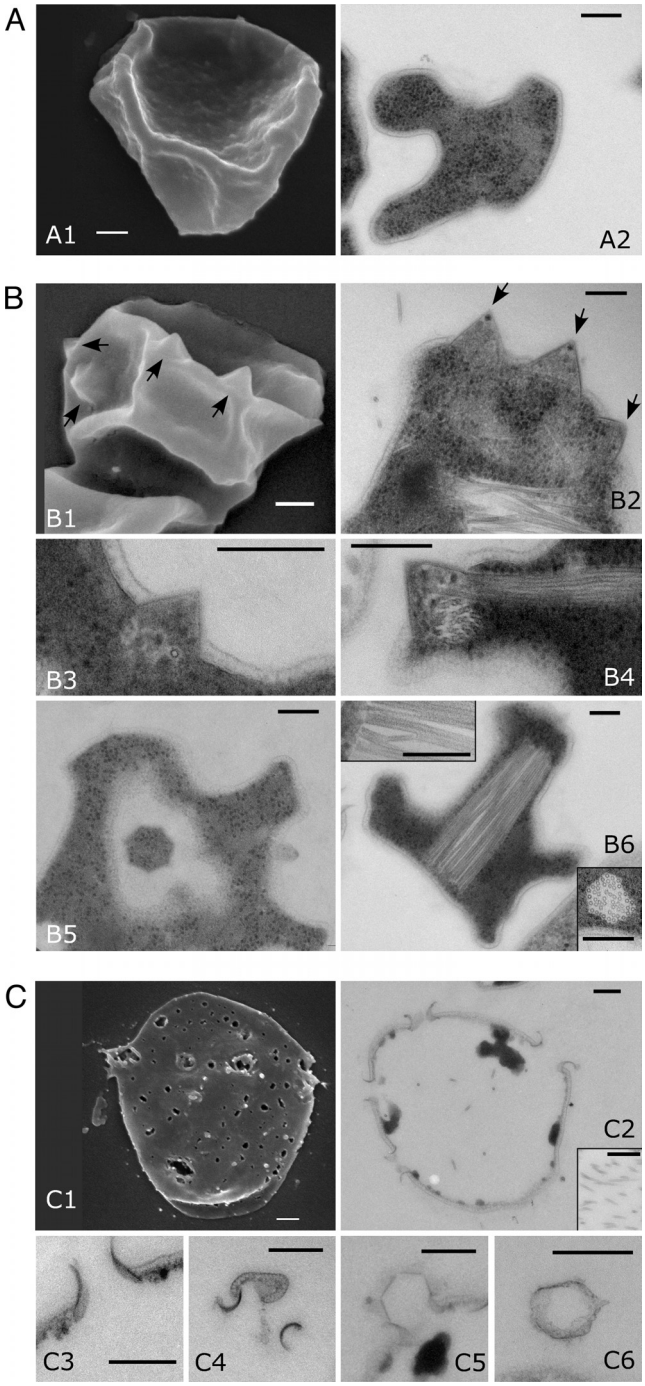

Fig. 4. VAPs, detected by SEM and TEM on SIRV2 infected *Sulfolobus* cells. *A1*, *B1*, and *C1* micrographs were obtained by SEM, all other micrographs are TEM images from thin sections. (*A*) Uninfected cells. (*B*) Cells 10 h after infection. (*B2*, *B3*, *B4*, and *B6*) Thin sections in a plane perpendicular to the cell envelope. (*B5*) Thin section in a plane parallel to the cell envelope. (*B1* and *B2*) arrows indicate VAPs. (*B6 Insets*) Details of intracellular virion aggregates, sectioned according to a parallel (up) or perpendicular (down) plane. (*C*) Cells 26 h after infection. (*C2*, *C3*, and *C5*) Thin sections in planes perpendicular to the cell envelope. (*C5*) Disrupted VAP partly detached from cell envelope. (*C4* and *C6*) Thin sections of disrupted detached VAPs in different section planes. (*C2 Inset*) Virion remains inside a lysed cell. (Scale bars, 200 nm.)

a transient viral factory, consisting of the whole transformed infected cell.

Our results show that lytic cycles may be more common for crenarchaeal viruses than previously assumed (7) and that lytic properties may have been overlooked in other crenarchaeal viruses. The original notion that the carrier state host-virus relationship is dominant in crenarchaea was consistent with the suggestion that this lifestyle would provide a durable intracellular refuge for the virus population in the harsh physico-chemical conditions at which cultured representatives of the Crenarchaeota thrive (T ≈60–90 °C, pH ≈3.0–6.0). In contrast, our findings imply that virus particles can persist in such extreme ecosystems long enough to encounter a new host cell. The SIRV2 virions are well adapted to harsh environments, being extremely stable in various solvents and other inhospitable conditions (14, 28), and almost as stable at 80 °C as phages of mesophilic bacteria are at 37 °C (29). Geothermal environments are extremely heterogeneous, due to a variety of gradients, dynamic movements and changes over time, and viruses may be trapped and preserved for long time periods in different environmental refuges in the absence of potential hosts. Finally, the fact that virus particles are apparently able to travel across the globe (30–32) also suggests that they are robust to variable environmental conditions and display stability over very extended time periods in a variety of biotopes.

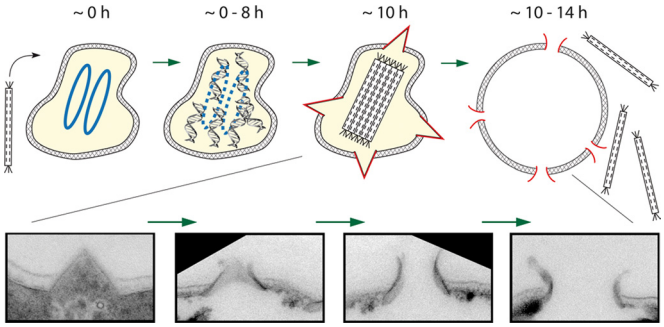

Fig. 5. Schematic representation of the major stages of SIRV2 infection cycle in the *Sulfolobus* host cell. Times after infection are indicated in hours. At 0 h, 2 chromosomes of *Sulfolobus* are shown in blue. Later between 0 and 8 h, they degrade concomitantly with viral DNA synthesis (gray helices). At 10 h, the VAPs (shown in red) and the intracellular clusters of assembled virions are shown. Finally, at time points between 10 and 14 h, the VAPs open (remains of VAPs shown in red), the cell lyses, and the virions are extruded. The gradual opening out of VAPs (at time points between 10 and 14 h) is illustrated in more details with fragments from the TEM of thin sections.

Materials and Methods

Virus, Host Strains, and Cultures. Virus stocks were prepared by PEG precipitation of the virions from the culture supernatants, followed by concentration and purification on Cesium chloride density gradients, as described in ref. 33.

The cells of *S. islandicus* LAL14/1 were grown in shaken 50-mL flasks at 78 °C, pH 3.0, in rich medium as described in ref. 14. Colonies were obtained on Gelrite plates as described in ref. 14. To infect cultures, the appropriate volume of virus solution was dialyzed against medium or water on 0.025- or 0.05-μm MF membrane filters (Millipore) and directly added to the liquid cultures during the early exponential phase ($OD_{600\ nm}$ between 0.09 and 0.25). For the time-course experiments [growth kinetics, flow cytometry, dot blot hybridization, and $DiBac_4$ (3) staining], all conditions were tested in triplicates. Six identical 50-mL cultures were launched by dilution of a same preculture. After overnight growth, SIRV2 was added to 3 of them at the appropriate m.o.i.

Titrations, OD, and Fluorescence Measurements. To determine CFU values, culture samples were submitted to serial dilutions and 5 μL of each dilution were spotted on plates. After incubation, the colonies were counted in the last or last 2 positive spots.

To determine the PFU values, the same method was used, except that 5 μL of each dilution were spotted on a fresh cell lawn. When required, the cells were removed by centrifugation before spotting. The cell lawns were prepared as described in ref. 11, using a soft Gelrite overlay. After incubation, single plaques were counted in the last or last 2 positive spots.

ODs were measured in 96-well round-bottomed culture microplates (TPP) in a

Multiskan Ascent microplate photometer (Thermo LabSystems) at 595 nm, using 200 μL of the culture.

Flow Cytometry. Sampling and flow cytometry were performed as described in ref. 19; the cells were fixed in 70% (vol/vol) ethanol and the intracellular DNA was stained with mithramycin A and Etd bromide. Samples were analyzed in a A40 Analyzer (Apogee, 25 mW solid-state laser, 405 nm wavelength). *S. islandicus* cell cycle was characterized preliminarily to the study of infected cultures (Fig. S4 and Fig. S5).

For the study of infected cultures, a high moi was used (≈10–15) to obtain as synchronous an infection as possible. At each time point, $OD_{595\ nm}$ was measured and CFU titers were determined to control that the usual growth pattern was obtained.

The distinct cell populations were identified based on the cell size distributions, DNA content distributions and 2D diagrams of cell size and DNA content. The data were gated, and several contours tested, to ensure the robustness of the analysis and of the identified cell populations. The proportion of empty cells over time was computed by gating the 2-D diagrams, similar to what is shown in Fig. S6. In Fig. 3*A*, the total percentage of chromosome-less cells in the culture is shown. In Fig. 3*B*, for the curve related to chromosome-less cells, the difference between the values at time points T and T-1 is plotted, reflecting the production of empty cells between 2 successive time points.

Dot Blot Hybridization. Cells were washed once in cold medium, pelleted by low-speed centrifugation, and stored at −20 °C until further use. Cell pellets were resuspended in Tris-acetate pH 6.0 precooled at 4 °C. The suspension volume was adjusted for cell concentration to be roughly constant in all samples, on the basis of OD measurements. Four microliters of each sample were spotted on Hybond-*n* + nylon membranes (Amersham Biosciences). The membranes were further prepared as for colony hybridization (34).

The probes were generated by PCR. An ≈240bp SIRV2 DNA fragment was generated using primer combination [5′-ACATGAAAAGTTAGAGAGATACAAACG(3872) 5′-TGGTTACCACTAGCTTCGCTAC(4086)] and a 1,300-bp fragment of the 16S rDNA of *S. islandicus* LAL14/1 was generated by using primers 8aF and 1512uR (35). The probes were [^{32}P]-end-labeled with EasyTide [α-^{32}P]-dATP (PerkinElmer) using a random-primed DNA labeling Kit (Roche Applied Science), according to the manufacturer's instructions.

All hybridization steps were performed at 65 °C in prewarmed solutions. After a minimum of 2 h prehybridization followed by overnight hybridization, both performed in Church Buffer [7% SDS (wt/vol), 0.5 M sodium phosphate, pH 7.2, and 1 mM EDTA], membranes were washed 2 times for 15 min in a solution of 2× SSC and 0.1% SDS, and 2 times for 15 min in a solution of 0.5× SSC and 0.1% SDS.

Membranes were exposed on a GP Phosphor Screen (Amersham Biosciences). The screen was scanned in a Molecular Dynamics Storm 860 (Amersham Biosciences). The images were analyzed with the ImageQuantTL software (Amersham Biosciences). After contrast and brightness adjustment, the radioactivity of each spot on the membranes was quantified, using the background removal option (local average). The images of Fig. 3 *D* and *E* were processed with ImageQuantTL for contrast and brightness adjustment and with ImageJ software (http://rsbweb.nih.gov/ij/) for background removal, using the ''sliding paraboloid'' function.

Transmission Electron Microscopy. Cells were pelleted by low speed centrifugation. The cell pellet was fixed overnight at 4 °C with 2.5% (wt/vol) glutaraldehyde in 20 mM Tris-acetate, pH 6, buffer, postfixed for 1 h in 1% (wt/vol) OsO_4, and dehydrated in a graded series of ethanol dilutions (25% (v/v) to 100% (v/v)). The cells were embedded in an epoxy resin which was polymerized at 60 °C for 48 h. Ultrathin sections (≈60 nm) were cut on a Leica Ultratuc UCT microtome and deposited on carbon-coated copper grids. They were stained for 30 min with 2% (wt/vol) uranyl acetate and for 5 min with 2.5% (wt/vol) lead citrate.

The grids were examined under a JEOL JEM-1010 transmission electron microscope operated at 80 kV. Images were recorded using an Eloise Keen View camera and the Analysis Pro software version 3.1 (Eloïse SARL).

Scanning Electron Microscopy. Cells were pelleted by low-speed centrifugation and fixed overnight at 4 °C with 2.5% (wt/vol) glutaraldehyde in 0,1 M Tris buffer, pH 6. Cells were adsorbed to polylysine-coated coverslips and postfixed 1 h in 1% (w/v) OsO_4 solution. Samples were dehydrated through a graded series of ethanol dilutions (25% (v/v) to 100% (v/v)) and critical point dried using a Leica EM CPD030 device. The dried coverslips were sputtered with 15-nm gold palladium in a GATAN Ion Beam Coater before examination with a JEOL JSM-6700F field emission scanning electron microscope operated at 5 kV. Images were acquired from the upper SE detector (SEI).

Note Added in Proof. At the final stage of preparation of the present publication, a detailed description of the findings reported in ref. 23 was published (36).

ACKNOWLEDGMENTS. We thank Dr. Soizick Lucas-Staat for great help in virus preparation, Léa Lepelletier for assistance in optical microscopy, and Professor Ryland F. Young for enlightening discussions. This work was supported by Ecole Nationale des Ponts et Chaussées, Agence Nationale de la Recherche (France), Swedish Research Council, and a grant from the Swedish Research Council for Environment, Agricultural Sciences and Spatial Planning (Formas).

1. Prangishvili D, Forterre P, Garrett RA (2006) Viruses of the Archaea: A unifying view. *Nat Rev Microbiol* 4:837–848.
2. Prangishvili D, Basta T, Garrett RA (2008) Crenarchaeal viruses: Morphotypes and genomes. *Encyclopedia of Virology*, eds Mahy BWJ, van Regenmortel MHV (Elsevier, Oxford), pp 587–595.
3. Prangishvili D, Garrett RA, Koonin EV (2006) Evolutionary genomics of archaeal viruses: Unique viral genomes in the third domain of life. *Virus Res* 117:52–67.
4. Janekovic D, et al. (1983) TTV1, TTV2 and TTV3, a family of viruses of the extremely thermophilic, anaerobic, sulfur reducing archaebacterium *Thermoproteus tenax*. *Mol Gen Genet* 192:39–45.
5. Prangishvili D, et al. (2006) Structural and genomic properties of the hyperthermophilic archaeal virus ATV with an extracellular stage of the reproductive cycle. *J Mol Biol* 359:1203–1216.
6. Ortmann AC, et al. (2008) Transcriptome analysis of infection of the archaeon Sulfolobus solfataricus with Sulfolobus turreted icosahedral virus. *J Virol* 82:4874–4883.
7. Prangishvili D, Garrett RA (2005) Viruses of hyperthermophilic Crenarchaea. *Trends Microbiol* 13:535–542.
8. Schleper C, Kubo K, Zillig W (1992) The particle SSV1 from the extremely thermophilic archaeon Sulfolobus is a virus: Demonstration of infectivity and of transfection with viral DNA. *Proc Natl Acad Sci USA* 89:7645–7649.
9. Vestergaard G, et al. (2005) A novel rudivirus, ARV1, of the hyperthermophilic archaeal genus Acidianus. *Virology* 336:83–92.
10. Contursi P, et al. (2006) Characterization of the Sulfolobus host-SSV2 virus interaction. *Extremophiles* 10:615–627.
11. Prangishvili D, et al. (1999) A novel virus family, the Rudiviridae: Structure, virus-host interactions and genome variability of the sulfolobus viruses SIRV1 and SIRV2. *Genetics* 152:1387–1396.
12. Rice G, et al. (2001) Viruses from extreme thermal environments. *Proc Natl Acad Sci USA* 98:13341–13345.
13. Vestergaard G, et al. (2008) Stygiolobus rod-shaped virus and the interplay of crenarchaeal rudiviruses with the CRISPR antiviral system. *J Bacteriol* 190:6837–6845.
14. Zillig W, et al. (1994) Screening for *Sulfolobales*, their plasmids and their viruses in Icelandic solfataras. *System Appl Microbiol* 16:609–628.
15. Peng X, et al. (2001) Sequences and replication of genomes of the archaeal rudiviruses SIRV1 and SIRV2: Relationships to the archaeal lipothrixvirus SIFV and some eukaryal viruses. *Virology* 291:226–234.
16. Bernander R (2007) The cell cycle of Sulfolobus. *Mol Microbiol* 66:557–562.
17. Duggin IG, Bell SD (2006) The chromosome replication machinery of the archaeon Sulfolobus solfataricus. *J Biol Chem* 281:15029–15032.
18. Barrangou R, et al. (2007) CRISPR provides acquired resistance against viruses in prokaryotes. *Science* 315:1709–1712.
19. Bernander R, Poplawski A (1997) Cell cycle characteristics of thermophilic archaea. *J Bacteriol* 179:4963–4969.
20. Wang IN, Smith DL, Young R (2000) Holins: The protein clocks of bacteriophage infections. *Annu Rev Microbiol* 54:799–825.
21. Bernhardt TG, Wang IN, Struck DK, Young R (2002) Breaking free: ''Protein antibiotics'' and phage lysis. *Res Microbiol* 153:493–501.
22. Miller S, Krijnse-Locker J (2008) Modification of intracellular membrane structures for virus replication. *Nat Rev Microbiol* 6:363–374.
23. Fulton J, et al. (2009) Genetics, biochemistry and structure of the archaeal virus STIV. *Biochem Soc Trans* 37:114–117.
24. Novoa RR, et al. (2005) Virus factories: Associations of cell organelles for viral replication and morphogenesis. *Bio Cell* 97:146–172.
25. Fontana J, Lopez-Montero N, Elliott RM, Fernandez JJ, Risco C (2008) The unique architecture of Bunyamwera virus factories around the Golgi complex. *Cell Microbiol* 10:2012–2028.
26. Claverie JM (2006) Viruses take center stage in cellular evolution. *Genome Biol* 7:110.
27. Raoult D, Forterre P (2008) Redefining viruses: Lessons from Mimivirus. *Nat Rev Microbiol* 6:315–319.
28. Steinmetz NF, et al. (2008) Site-specific and spatially controlled addressability of a new viral nanobuilding block: *Sulfolobus islandicus* rod-shaped virus 2. *Adv Funct Mater* 18:1–9.
29. De Paepe M, Taddei F (2006) Viruses' life history: Towards a mechanistic basis of a trade-off between survival and reproduction among phages. *PLoS Biol* 4:e193.
30. Breitbart M, Miyake JH, Rohwer F (2004) Global distribution of nearly identical phage-encoded DNA sequences. *FEMS Microbiol Lett* 236:249–256.
31. Sano E, Carlson S, Wegley L, Rohwer F (2004) Movement of viruses between biomes. *Appl Environ Microbiol* 70:5842–5846.
32. Snyder JC, et al. (2007) Virus movement maintains local virus population diversity. *Proc Natl Acad Sci USA* 104:19102–19107.
33. Bettstetter M, Peng X, Garrett RA, Prangishvili D (2003) AFV1, a novel virus infecting hyperthermophilic archaea of the genus acidianus. *Virology* 315:68–79.
34. Sambrook J, Fritsch EF, Maniatis T (1989) *Molecular Cloning: A Laboratory Manual* (Cold Spring Harbor Lab Press, Plainview, NY), 2nd Ed.
35. Eder W, Ludwig W, Huber R (1999) Novel 16S rRNA gene sequences retrieved from highly saline brine sediments of kebrit deep, Red Sea. *Arch Microbiol* 172:213–218.
36. Brumfeld SK, et al. (2009) Particle assembly and ultrastructural features associated with replication of the lytic archaeal virus Sulfolobus turreted icosahedral virus. *J Virol* 83:5964–5970.